Hydrogeology Journal
DOI 10.1007/s10040-014-1195-0

Numerical modeling of salinity distribution and submarine groundwater discharge to a coastal lagoon in Denmark based on airborne electromagnetic data

Kinza Haider · Peter Engesgaard · Torben Obel Sonnenborg · Casper Kirkegaard

Abstract The beneficial use of large-scale geophysical surveys in combination with numerical modeling for assessing water resources problems in coastal areas is demonstrated. A 5,000-year long historical evolution of the regional distribution of salinity beneath a coastal lagoon in Denmark is simulated in a stage-wise approach using a two-dimensional variable-density flow and transport model and compared with an interpreted resistivity distribution from transient electromagnetic data. A sequence of multi-layer unconfined/confined aquifers with non-continuous aquitards is needed to match observations in terms of complexity in resistivity/salinity distribution, deep-seated low resistivity zones (trapped residual saltwater), and presence of groundwater discharge tubes with high resistivities indicating both near and off-shore discharge of fresh groundwater. Refreshening of the lagoon system is ongoing and simulations show that this process has been most rapid during the last ~300 years, but will continue at a slower rate for the next many hundreds of years. The development of the lagoon over the last 5,000 years, the associated changes in salinity and the present-day control of lagoon salinity are responsible for these processes. Finally, simulation results show that the groundwater influx to the lagoon is significant. The estimated fluxes correspond to 168 % of net precipitation on the lagoon or 17 % of the discharge from the largest river into the lagoon.

Keywords Coastal lagoon · Submarine groundwater discharge · Geophysical methods · Numerical modeling · Denmark

Received: 15 December 2013 / Accepted: 3 September 2014

K. Haider (✉) · P. Engesgaard
Department of Geosciences and Natural Resource Management, University of Copenhagen, Øster Voldgade, 10, 1350 Copenhagen, Denmark
e-mail: kinza.haider@hotmail.com
Tel.: +45 50299000

T. O. Sonnenborg
Department of Hydrology,
Geological Survey of Denmark and Greenland, Øster Voldgade, 10, 1350 Copenhagen, Denmark

C. Kirkegaard
Department of Geoscience,
Aarhus University, C.F. Møllers Allé, 4, 8000 Aarhus, Denmark

Introduction

Lagoons are brackish water bodies of concave shape that develop at coastlines due to sedimentary transport plus accumulative and erosive wave action. Long-shore drift processes carry and deposit sediments across the mouth of the lagoon, over time isolating it from the sea. Lagoons cover about 13 % of the world's coastlines and lagoon areas provide the sites of fastest human development (Santos et al. 2008). Such natural habitats face potential climate change and increasing pressure on sparse groundwater resources. Hence, it is obviously of vital importance to understand the groundwater dynamics and interaction with the lagoon. The water balance and ecology of lagoons is complex, depending on fluxes from not only groundwater, but also river inlets, precipitation, storm-events and any associated nutrients/contaminants (Carter et al. 2008). It is therefore important to understand both the temporal and spatial impacts of natural and anthropogenic changes to all of these flux components of which groundwater can be the most difficult one to quantify (Burnett et al. 2006a, b; Spruill and Bratton 2008; Stieglitz et al. 2008). Groundwater discharge (GWD) or rather Submarine Groundwater Discharge (SGD) to coastal lagoons is often an overlooked component in the water budget (Burnett et al. 2006b) bringing in nutrients or contaminants (Andersen et al. 2007; Kaleris et al. 2002; Langevin 2003). Some of the known hydrogeological driving forces for SGD are topography and inland hydraulic gradients, density gradients, seawater recirculation, and geothermal convection (Wilson 2005). SGD is mainly restricted to locations near the shoreline with occasional far-offshore discharge up to several kilometers from the shoreline as a result of leaks/escapes from confined aquifers (Manheim et al. 2004; Thompson et al.

Published online: 21 September 2014

2007). However, the relative importance of such off-shore discharge is poorly understood.

Lagoons are generally isolated from the sea by either natural barriers or in a few marginal cases by manmade islands, providing protection from tidal effects and potentially causing a shift in salinity towards more brackish levels. Such a shift can be caused by a continuous influx of surface-water/groundwater from the mainland, effectively decreasing salinity in the lagoon over time. In cases where decreasing salinity levels have undesirable side effects such as eutrophication, it is sometimes possible to adequately control the system by construction of sluices or gates. As such, lagoon salinity can be affected by both controlled input of seawater, season-dependent discharge from inland rivers and direct groundwater discharge. Coastal lagoons thus essentially behave like lakes of brackish water with varying salinity, interacting with the groundwater in adjacent aquifers.

Understanding the formation of lagoons over time is one of the keys to determine the salinity distribution in these environments. A few studies have recently focused on the analysis of past characteristics to define current observations. Based on geological, chemical, isotopic and geophysical data, Post et al. (2003) explained the origin of brackish to saline groundwater in the coastal area of the Netherlands by Holocene transgressions. This led to an understanding of salinization mechanisms in relation to the paleogeographical development and the occurrence of low-permeability strata during the Holocene. In another study, Post et al. (2013) uses numerical modeling to examine the influence of mixing and a selection of other hydrogeological factors on steady-state age distributions of groundwater in coastal aquifers. Vaeret et al. (2012) studied the effects of Holocene dynamics in the saltwater–freshwater interface in response to sea-level fluctuations using a numerical model. Their transient model reflects the concept of moving from a one-island concept, as seen today, to a multi-island concept during sea-level high stands which explains the reduction of freshwater input due to a decrease in surface area for recharge. It is concluded from these studies that the age of groundwater in coastal aquifers is related to the dispersive density-dependent flow and transport. In another study, Cohen et al. (2010) examined the presence of freshwater sequestered within permeable, porous sediments beneath the Atlantic continental shelf of North and South America. According to the hypothesis, this freshwater emplacement occurred during Pleistocene sea-level low stands when the shelf was exposed to meteoric recharge and by elevated recharge in areas overrun by the Laurentide Ice Sheet at high latitudes. They used results from a high-resolution paleohydrologic model of groundwater flow, heat and solute transport, ice sheet loading, and sea-level fluctuations for the continental shelf from New Jersey to Maine over the last 2 million years to test the hypothesis. Their analysis suggests the presence of fresh to brackish water within shallow Miocene sands more than 100 km offshore of New Jersey, which is facilitated by discharge of submarine springs along Baltimore and Hudson Canyons where these shallow aquifers crop out.

As the recognition of the significance of SGD has grown, many studies have appeared during the last decade using different investigation techniques, standalone or in combination. Three approaches to assess SGD can be direct measurements, tracer techniques, or modeling (Burnett et al. 2001). Langevin (2003) simulated SGD to a marine estuary using variable density groundwater flow modeling for understanding complex groundwater flow processes in coastal environments. Thompson et al. (2007) simulated SGD and salinity distribution covering the continental shelf at a regional-scale. Their results on discharge were in good agreement with observations from a geochemical tracer study. Carter et al. (2008) simulated average position of the freshwater–brackish water interface using a steady-state groundwater model that compared well with observed electrical resistivity images in a tidal salt marsh basin of an estuarine environment. Robinson et al. (2006) identified processes that affect the groundwater flow dynamics and pattern of salinity distribution in a subterranean estuary using numerical modeling and salinity as a tracer. However, very few of these studies have accounted for multiple aquifer systems and have not addressed salinity distribution changes as a result of groundwater flow from deeper aquifers. Moreover, field observations were generally not available at large scales (10s of kilometers).

Recently, geophysical investigation techniques such as airborne electromagnetic surveys, marine electrical resistivity imaging, and ground electrical resistivity surveys have gained popularity as a way of mapping SGD and salinity distribution. These methods are not only helpful in understanding SGD patterns and saltwater intrusion in coastal environments, but also help in delineating geological heterogeneity at very high spatial resolution. Vrbancich (2009) mapped the salinity distribution and sediment thickness at a bay using airborne electromagnetic cross-sectional survey across areas ranging from 3×0.06 to 8×0.1 km^2. Viezzoli et al. (2010) found airborne electromagnetic surveys to be a powerful tool for the hydrogeological characterization of large fresh–salty transitional environments such as wetlands, lagoons, and deltas at large scales. They were able to map the salinity distribution and identify areas of discharge. Stieglitz et al. (2008) found that an improved spatial distribution of SGD could be derived using ground electrical resistivity surveys in combination with hydrogeological investigative methods at small scales (~100 m^2). Manheim et al. (2004) used streamer electrical resistivity surveys to recover information required for hydrologic modeling of shallow coastal aquifer systems and discharge into both onshore and far offshore areas at very large scales (>20 km). They were also able to develop conceptual models showing patterns of paleo-drainage and subsequent development of the groundwater flow regime. Such studies show that hydrogeophysical investigations in combination with hydrogeological techniques have proven their worth in

DOI 10.1007/s10040-014-1195-0

understanding salinity distribution and heterogeneity at both large and small scales and how it may affect SGD.

The main objective of this study is to investigate the impact of groundwater flow of a multi-layer aquifer system on the historic evolution of salinity distribution and submarine groundwater discharge to a coastal lagoon. To achieve this objective, results from an airborne geophysical survey and 2D numerical variable-density groundwater flow and transport modeling are combined for a coastal lagoon at the Western coast of Denmark. The model is used to quantify present-day fluxes of submarine groundwater discharge into the lagoon and compare these with other inputs. Finally, the model is used to predict future long-term changes in the salinity distribution.

Site description and background

The study area consists of a bar-built estuary, also referred to as a lagoon system, named Ringkøbing Fjord in Western Jutland, Denmark (Fig. 1), which is separated from the North Sea by the Holmsland Barrier. This barrier is primarily built up of sequences of wash over deposits, locally interspersed with eolian deposits (Anthony and Moller 2002). The lagoon has an area of approximately 300 km^2 with around 110-km-long coastline. The water depth is relatively shallow near the shoreline (<0.5 m) and the surrounding land surface elevation is below 10 m above sea level. Details of the bathymetry and water levels can be found in Nielsen et al. (2005). The lagoon is connected to the North Sea in the west through a sluice at Hvide Sande. The sluice acts as a 'control gate' of incoming seawater and is operated to keep the water level of the lagoon not more than 0.25 m above sea level and the salinity between 6 and 15 ‰ (Nielsen et al. 2005). A monitoring station in the North Sea off-shore the coast of the barrier measures salinity between 24 and 34 ‰. Maximum and minimum salinities are observed in summer (July) and winter (January), respectively, both in the lagoon and seawater due to higher input of freshwater in winter (wet season) and vice versa in summer. Skjern River discharges to the lagoon at the south-eastern shoreline.

Formation of the lagoon

During the late Weichselian, large outwash plains covered this area, infilling and locally eroding the existing landscape leaving buried valleys with sub-glacial melt water deposits (Anthony and Moller 2002). The outwash plains were gradually submerged below sea level during the Holocene transgression causing the upper part of the glacio-fluvial sediments to be reworked and redistributed by coastal and marine processes. A study conducted by Johansen (1913) is the only one that looks at the situation up to 1913 in Ringkøbing Fjord. Johansen (1913) explains that approximately 5,000 years ago, the coastline was situated at what is now the eastern shoreline of the lagoon and the lagoon was part of the North Sea (likely with a much higher salinity than presently; Fig. 2a). Due to sediment transport processes, Holmsland Barrier was slowly formed parallel to the west coast of Denmark until ~18th century (Fig. 2b). The formation of this barrier isolated the lagoon from the North Sea, resulting in significant reductions in salinity (average of 9 ‰) (Johansen 1913). Over a couple of hundred years, gradual sedimentation of the outlet and subsequent bar breaching in connection with storms in the North Sea caused dramatic changes to the physical and biological conditions in and around the lagoon. The Hvide Sande sluice was therefore constructed in 1931 in order to control the water level and salinity of the lagoon (Fig. 2c). However, the salinity of the now isolated lagoon was reduced to ~6 ‰ causing eutrophication problems. Finally, in the late 1980's, it was decided to raise the salinity levels and keep the salinity between 6 and 15 ‰ by controlling the seawater input to the lagoon (Fig. 2d).

Regional and local geology

At a regional scale, the lagoon is geologically a part of the Ringkøbing-Fyn High, which forms an east–west-striking system of highs running across Denmark and the North Sea area. As part of an airborne geophysical study that the present paper builds upon, Kirkegaard et al. (2011) review available background information on the area and describe how the setting is well understood and composed of three major sequences. Starting from the bottom: (1) a deep marine Paleogene clay of very low resistivity (1-5 Ohm.m; Jørgensen et al. 2005) situated at depths of around 300 m (Friborg and Thomsen 1999); (2) alternating layers of Miocene sand, silt, and clay (Rasmussen 2004; Scharling et al. 2009) with resistivities above 20–30 Ohm.m for non-saline pore water (Jørgensen and Sandersen 2009), and (3) a relatively thin surface sheet (typically 10–20 m) of glacial sediments with resistivities above 100–200 Ohm.m for the case of fresh pore water (Jørgensen and Sandersen 2009). Buried tunnel valleys incising the Miocene are also known to be found in the area (Jørgensen and Sandersen 2006), located mostly in the western part of the survey area of Kirkegaard et al. (2011). The position of one of these buried valleys coincides with the position of one of two deep drillings marked in Fig. 1. These two boreholes are also almost coincident with a flight line of the survey by Kirkegaard et al. (2011), thus providing data for direct comparison between geophysics and geology. Borehole DGU 93.1125 is a 170-m-deep drilling showing mostly fine sand but with clay layers located at depths of 10–16, 26–38, 60–91, 106–131, and 158–169 m. These clay layers indicate the presence of a four-aquifer system up to a depth of around 200 m east of the lagoon. DGU 92.81 is a 91 m deep borehole characterized by only medium Quaternary sands of glacial melt-water origin showing possible incision of a buried valley around this location at the Holmsland Barrier. A few other shallow and deep boreholes on Holmsland Barrier also record medium Quaternary sands in their entire column.

 DOI 10.1007/s10040-014-1195-0

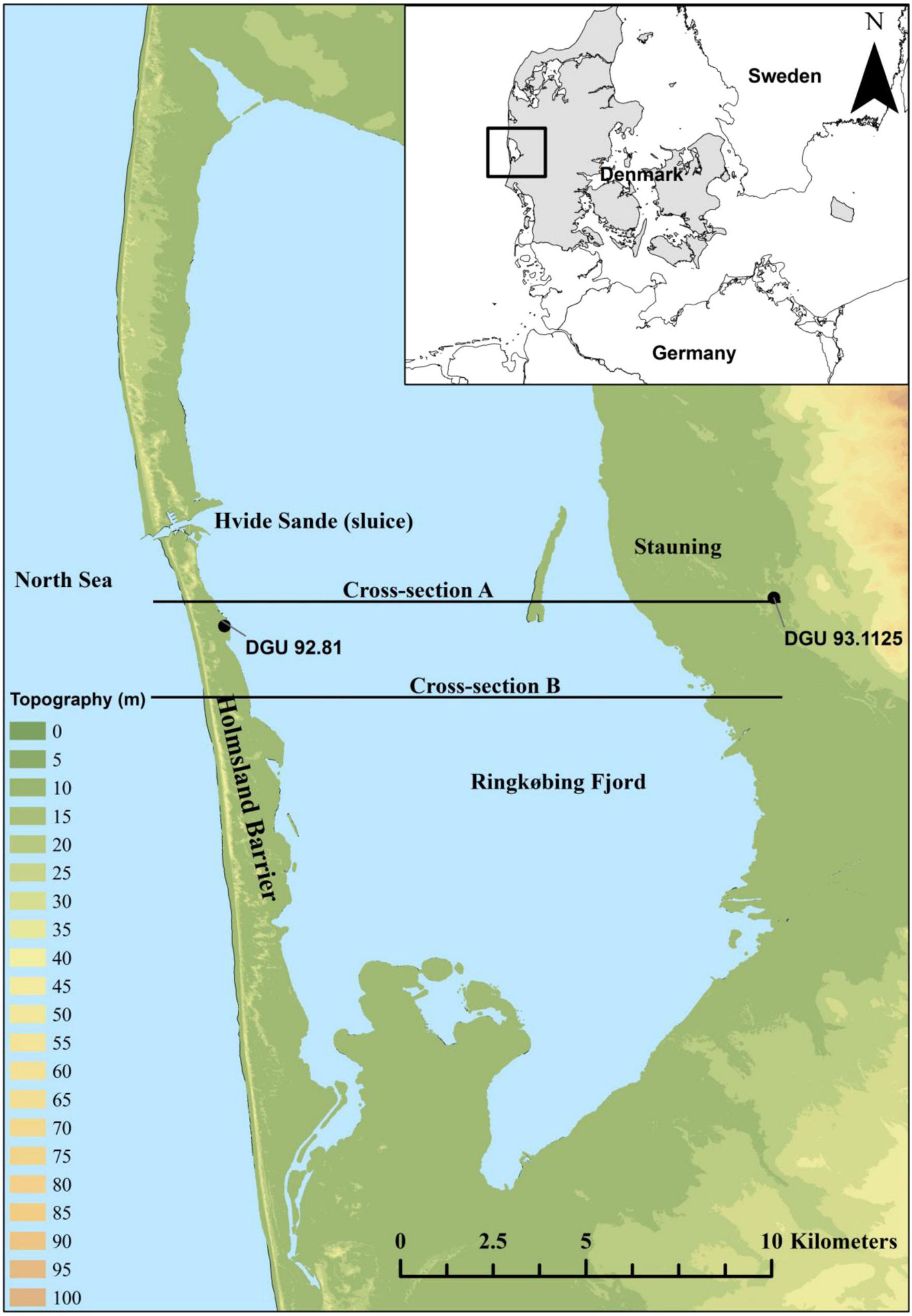

Fig. 1 The study area in Denmark, with the *North Sea* in the west, *Stauning* town in the East, *Holmsland Barrier* between *Ringkøbing Fjord* and *North Sea*, and with *Hvide Sande sluice* in the northwest. Geophysical survey area lines are highlighted as cross-section '*A*' and '*B*' in *black*. *Black circles* indicate the location of deep boreholes DGU 93.1125 and DGU 92.81. Topography is in meters above sea level (m asl)

DOI 10.1007/s10040-014-1195-0

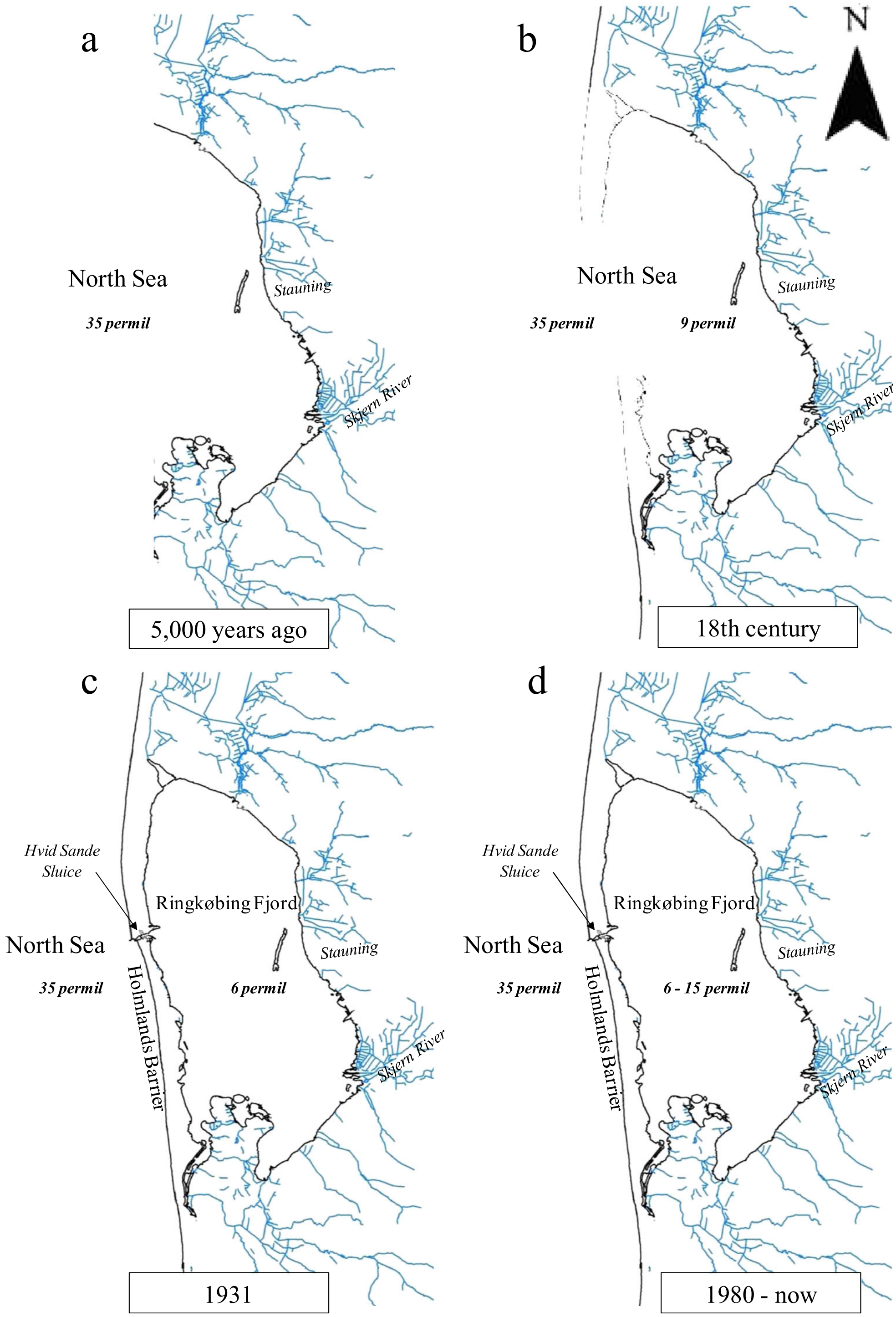

Fig. 2 Hypothetical evolution of the lagoon showing shifts of sea shoreline and salinity. **a** Stage I, 5,000 years ago with sea coastline adjacent to landside with a salinity of 35 ‰; **b** Stage II, dates back to 18th century when Holmsland Barrier was formed thereby indirectly causing dilution of salinity in the water surrounding landside (9 ‰) due to runoff from catchments and groundwater; **c** Stage III, ~ 1931 shows time when salinity in the lagoon lowered to 6 ‰ due to complete formation of Holmsland Barrier (at this time it was decided to construct the Hvide Sande sluice); **e** Stage IV, 1980 until today shows the current monitored and controlled salinity levels of the lagoon. Skjern River is also shown in the southeast. Figure is not to scale

Hydrology and hydrogeology

The catchment area to Ringkøbing Fjord is 3,500 km^2, with two small streams and one main river, Skjern, discharging into the lagoon. Mean annual precipitation to the catchment is estimated as 1.05 m/year whereas average potential evapotranspiration is 0.57 m/year (Stisen et al. 2011). Annual mean outflow from Skjern River, and average precipitation into and evaporation from the lagoon are about 40, 10, and 6 m^3/s, respectively.

DOI 10.1007/s10040-014-1195-0

The groundwater system consists of an upper shallow unconfined aquifer and a series of confined aquifers. Based on land surface elevations and hydraulic head data in the unconfined aquifer, a water divide is expected around 3 km inland from the shoreline into the study area. Hydraulic head measurements in the catchment show groundwater flow into the lagoon, i.e., from east to west. Well DGU 93.1125, located ~4 km east of the lagoon, is screened at two levels: in the top unconfined aquifer showing a hydraulic head of ~3 m and at a depth of 150 m with a hydraulic head of ~6.5 m. This means that the head in the deeper aquifer is higher than in the shallow aquifer. The head values vary seasonally by about 1 m in the unconfined aquifer. On the Holmsland Barrier on the western side of the lagoon, well DGU 92.81 has a hydraulic head of ~0 m at a depth of 85 m, i.e., close to sea level. Hydraulic conductivities for the major sand units have been estimated to 40–60 m/d, whereas values for Quaternary clays between 0.02 and 0.06 m/d have been found through calibration of a hydrological model covering the entire Skjern River catchment (Stisen et al. 2011).

Methods

Airborne geophysical survey

In August 2008 an airborne geophysical transient electromagnetic (TEM) survey was carried out in the lagoon area (Kirkegaard et al. 2011) using a high-resolution SkyTEM instrument (Sørensen and Auken 2004). The Kirkegaard et al. (2011) study is essential to this hydrological investigation, so this section presents a summary of the premise by which Kirkegaard et al. (2011) interpret their resistivity model, and further presents their most important results (for the full methodological details, refer to the original paper).

Inductive geophysical instruments, such as SkyTEM, are particularly sensitive to electrically conductive targets, making them very useful for investigating settings of varying water salinity. For the studied survey area, the overall geological setting is already well understood, as discussed in section 'Regional and local geology'; the only low-resistivity geological unit (<20–30 Ohm.m) known to reside in the area is located well below the SkyTEM instrument's depth of investigation. This greatly simplifies the interpretation of the resistivity model, since it implies that any structures of low resistivity can be directly linked to the presence of saline water: lower resistivity implying higher salinity. Deriving exact relations between measured resistivity and groundwater salinity is complicated in general and far beyond the scope of this interpretation. For the purposes of the present study, however, only different characteristic levels of salinity need to be discriminated corresponding to different characteristic levels of resistivity. Within the investigated area there are different distinct salinity levels in the seawater of the North Sea (~33 g/L), brackish water in the fjord (~15 g/L) and freshwater discharging into the fjord (~0 g/L). The lowest subsurface resistivity of the obtained resistivity model is found in the buried valleys, with a characteristic resistivity level around 1.75 Ohm.m. This resistivity value is so low that it is very difficult to explain by anything but the presence of saline water from the North Sea, in particular since the core of the DGU 92.81 drilling clearly shows the valley infill consists of glacial sand. Assuming the buried valleys are indeed filled with water of the same salinity as in the North Sea, the formation factor of the infill sediments is found to be approximately 6. Assuming this factor is reasonably representative of the area as a whole, characteristic resistivity levels corresponding to distinct levels of salinity can be estimated. Formations saturated by saline water from the North seawater should appear with a characteristic resistivity of around 1.5–2 Ohm.m, while 3.5–4 Ohm.m should be found for sediments saturated by brackish lagoon water and a significantly higher resistivity should be observed for areas saturated by freshwater. While both geological background information and the geophysical model itself indicate a relatively homogenous setting, the provided estimates can obviously only be taken as guidelines for interpretation. A large local deviation in formation factor from the value of 6 could cause, e.g., saline water to show up near the estimated signature level of brackish water, but as salt is the only source of conductivity to be found in the area, it would not be possible to mistake saline/brackish water for freshwater or vice versa.

Regarding the resolution of the resistivity model itself there are different considerations in the vertical and horizontal direction. At the very near surface, the horizontal resolution of the resistivity model can be considered comparable to that of the sounding spacing, i.e. approximately 25 m. The horizontal model resolution effectively decreases with depth, as the volume probed by the TEM method can be visualized as a cone extending out beneath the instrument. Vertical model resolution is highly model dependent, with well-defined vertical layer interfaces of substantial resistivity contrast being the best-determined targets. For many sedimentary (quasi-layered) settings, it is possible to resolve both layer resistivities and interface depths within estimated uncertainties of 10–20 %, as long as the resistivity contrast is reasonably pronounced and the target is situated above the instrument's depth of investigation (DOI). The DOI is a robust measure of how deep the resistivity model can be trusted, based on calculation of the depth where the model-dependent sensitivity function drops below a global threshold. It is used to mask the model result at depth, in order not to draw any conclusions based on model parameters that the measured data do not provide any information on. The DOI concept is described in detail by Christiansen and Auken (2012) and for an in-depth discussion of the resolution of the TEM method, refer to Auken et al. (2008).

Numerical model

Two-dimensional (2D) cross-sectional numerical models were developed for variable-density-dependent flow and transport. The HydroGeoSphere code (HGS) was used for this purpose (Therrien et al. 2004). Important elements in the development of these models are the construction of conceptual models (as described in the results section) for the hydrogeology and salinity distribution based on the borehole and geophysical information. The historic evolution of salinity distribution and SGD has been simulated for the following three cases:

- Homogeneous geology (base case)
- Heterogeneous geology defined by the conceptual model A (Fig. 4a)
- Heterogeneous geology defined by the conceptual model B (Fig. 4b)

The homogeneous case has been included to investigate the relative importance of the multi-aquifer system in the heterogeneous cases on salinity distribution and SGD. This model was also used to perform a sensitivity analysis of the effects of uncertainty in dispersion and hydraulic conductivity parameters on the salinity distribution and to predict the future evolution of salinity.

The model domain is a rectangular 2D vertical cross section with 25,000 m length and 200 m depth with cell sizes 50 m long and 1 m wide. Boundary conditions are assigned with one historic shift in sea shoreline location, introduction of the lagoon and then two shifts in its salinity. Thus, the numerical modeling is divided into four stages. Stage I comprises a quasi-steady time period in which the seabed lies horizontally between 0 and 17,000 m, and land between 17,000 and 25,000 m, corresponding to Fig. 2a. In stages II, III, and IV, the sea is located according to present day as shown in Fig. 4. The simulation period is 300 years for stage II, 50 years for stage III, and 30 years for stage IV corresponding to Fig. 2b–d, respectively. The steady-state results of stage I were used as initial conditions for stage II, the final results of stage II were used as initial conditions for stage III, and so on. The vertical sea boundary (left face) was assigned a constant freshwater head of 0 m (sea level), increasing with increasing depth. Nodes representing the horizontal seabed were assigned a fixed freshwater head of 0 m. The lagoon boundary was assigned a fixed freshwater head of 0.2 m. Landside boundary (right face) was assigned fixed values of freshwater (or hydraulic head), corresponding to the respective aquifer systems for heterogeneous cases A and B (Fig. 4). Here, a hydraulic head of 8 m is assigned in the unconfined aquifer, which is approximately equal to the observed values in wells about 8 km from the lagoon shoreline. In the deeper aquifers, hydraulic heads were assumed to increase linearly so that the observed hydraulic head measurement at 150 m depth in borehole DGU 92.1125 approximately matches the boundary condition. The result is that the first confined aquifer was assigned a head of 8.5 m, the second confined aquifer a head of 9 m, and the third aquifer a hydraulic head of 9.5 m. The last two confined aquifers were assigned a head of 10 and 11 m, respectively (Fig. 4b).

In the homogeneous case, a constant hydraulic head of 8 m was used. The bottom boundary is specified as impermeable. Recharge based on results from an integrated hydrological model of the area (Stisen et al. 2011) of 0.48 m/year is applied to the Holmsland Barrier and east of the lagoon. A constant relative concentration of 1.0 equivalent to 1,025 kg/m^3 (35 ‰) and 0.0001 equivalent to 1,000 kg/m^3 were specified at the sea (maximum fluid density) and land (freshwater) boundaries, respectively. For the lagoon boundary, a constant relative concentration of 0.25 (9 ‰), 0.16 (6 ‰) and 0.4 (15 ‰) were assigned for stages II, III, and IV representing the different time periods shown in Fig. 2. The initial (t=0 d in stage I) freshwater head was 0.2 m, whereas the initial relative concentration was 1.0 between 0 and 17,000 m, and 0.00001 between 17,000 and 25,000 m. All concentration boundaries are first type specified concentration (Dirichlet). Porosity was assumed to be 0.3 representing both medium sand and clay. The horizontal hydraulic conductivity (K_x) for sand was 50 m/d, while clay layers in the heterogeneous cases had K_x of 0.4 m/d (Stisen et al. 2011). The infill of the buried valleys is assumed to be sand with the same hydraulic properties as the other sand aquifers. Vertical hydraulic conductivity was assumed as $0.1 \times K_x$. Longitudinal and vertical transverse dispersivities were taken as 25 and 2.5 m, respectively, for all cases. A sensitivity analysis is performed on dispersion parameters to evaluate the uncertainty of these on the results.

A Picard iteration criterion was defined, finding that the maximum relative change in concentration and hydraulic heads between subsequent iterations were smaller than 1 %. Steady state was assumed when solute concentrations converged to stable values in the transitional zone.

Results

Geophysical model

New interpretations of the salinity distribution of two cross-sections extracted from the resistivity model obtained from inversion of the original SkyTEM dataset are made. These particular cross sections were not analyzed in the study by Kirkegaard et al. (2011) and no assumptions were used about formation factor in the interpretations. The locations of the cross sections are marked in Fig. 1 and the resistivity cross-sections themselves are shown in Fig. 3. Cross-section A was selected to match the location of borehole DGU 92.1125 and cross-section B was chosen specifically to understand possible offshore discharge. Both cross-sections run west to east through the lagoon and extend a further 1–2 km inland and in to the North Sea. The DOI is marked with a black line in Fig. 3, which also features assumed groundwater streamlines, possible areas of offshore SGD, interpreted saltwater–freshwater interfaces, and further annotations of major features.

Figure 3 shows the resistivity distribution in both cross-sections. In the eastern part of the survey area, the setting is highly resistive all the way down to the DOI, implying that this area is fully saturated by fresh groundwater of terrestrial origin. At shallow depth, this

DOI 10.1007/s10040-014-1195-0

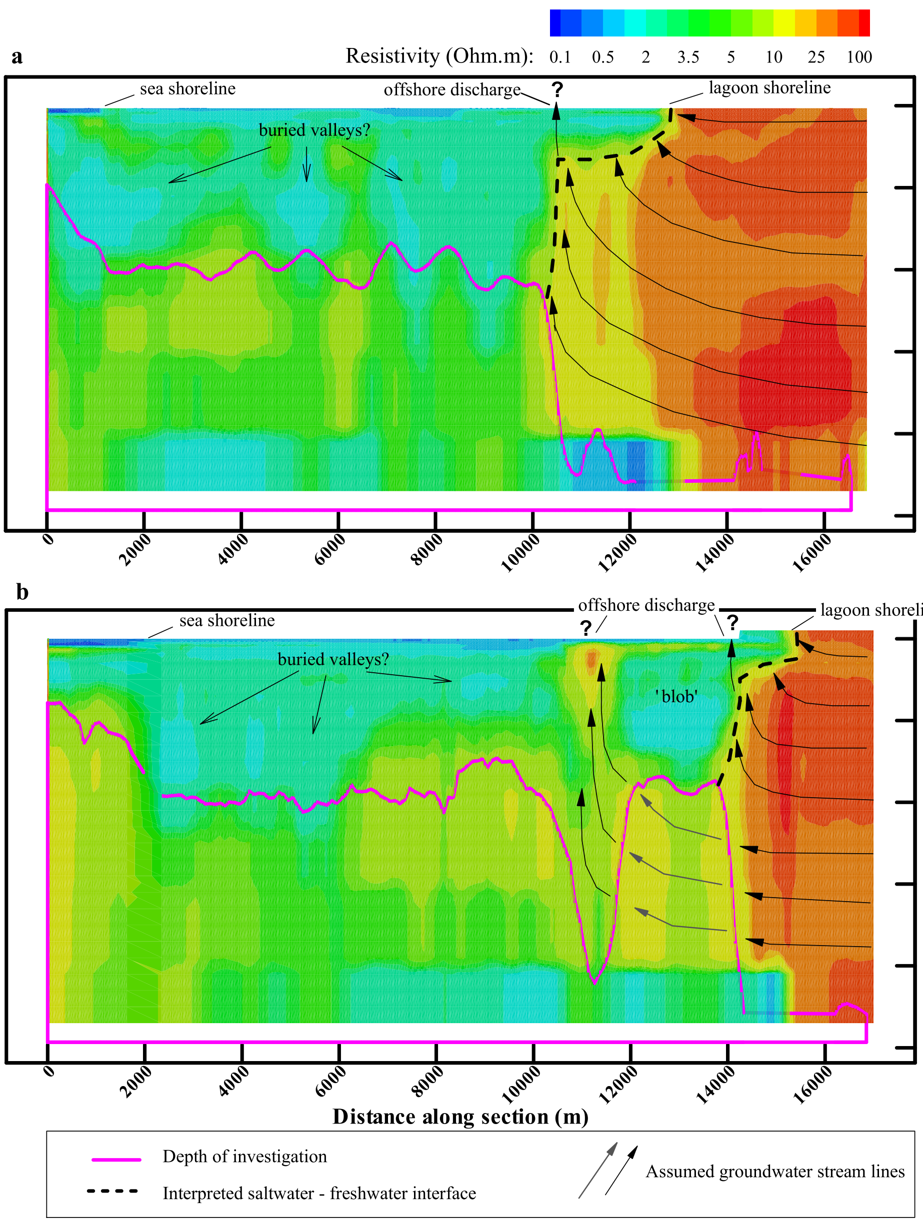

Fig. 3 2D resistivity inversion profiles (see Fig. 1 for locations) mapped by SkyTEM in Ringkøbing Fjord (August 2008), **a** cross-section A which lies adjacent to borehole DGU 93.1125 and **b** cross-section 'B'. *Gray line* represents lower limit of trustable depth of resistivity (DOI). *Solid arrowed lines* (*black* and *gray*) represent assumed flow path of groundwater, and *dashed lines* show expected brackish-water/groundwater interface; possible zones with offshore submarine groundwater discharge are marked as '*?*' and buried-valley incisions are indicated. The trapped old seawater '*blob*', interpreted as due to formation of the lagoon, is also highlighted

resistive zone ends right around the lagoon shoreline, whereas it extends further out at greater depths below the lagoon. In these deeper parts a transition zone of moderate to high resistivity exists (>15 Ohm.m, still characterized as freshwater), before the general resistivity pattern turns to lower values (<10 Ohm.m), indicating more saline water further away from the shoreline. In the western part of the survey area a resistivity level close to the signature level of brackish lagoon water is generally found, except for some possible intricate buried valley incisions whose resistivity suggest the presence of seawater. These positions are suggested to be places where Miocene clay layers may have been eroded by buried valley incisions, resulting in a short circuit of the shallow and deeper lying aquifer systems. Such a short circuit would allow saltwater to intrude to greater depths and the very low resistivity levels could then be explained by the presence of old seawater, located here since before the formation of the lagoon. It is noted that the model accurately recovers resistivities corresponding to the actual salinity levels of the surface water in both the North Sea and the lagoon itself.

In cross-section A specifically (Fig. 3a), relatively high resistivity indicates fresh groundwater extending out beneath the lagoon to a distance of roughly 2,500 m from the shoreline at depths of approximately 20–200 m. The

 DOI 10.1007/s10040-014-1195-0

interpreted brackish-water/freshwater interface, marked with a dashed line in the figure, is located further offshore due to a highly resistive zone in the deeper confined aquifer systems underneath the lagoon compared to the interface location in the shallow part. This indicates that groundwater is possibly present further offshore in deeper aquifers compared to shallow aquifers. Groundwater discharge is observed through the horizontal transition from high to low resistivity by the lagoon shoreline (marked by the saltwater–freshwater interface in Fig. 3a). However, it is clear that the exact width of this discharge zone is beyond what the SkyTEM instrument can resolve. A zone featuring lower resistivities extends upward to shallower depths indicating the location of potential offshore SGD, annotated with a question mark in Fig. 3a.

In cross-section B (Fig. 3b), a very high resistivity zone is again found in the upper part changing abruptly at the shoreline with this zone extending further out beneath the lagoon at greater depth similar to cross-section A. However, in this case, the freshwater indicated by this high resistivity zone only extends to around 1,000 m from the shoreline (coordinate 14,500–15,500 m). Further offshore, a zone of low resistivity is found down to the DOI (coordinate 12,000–14,500 m). The resistivity of this zone ('blob') decreases towards the center and reaches values around those characteristics for the buried valleys further to the west. Further offshore, around coordinate 11,500 m, a highly resistive zone is found suggesting strong groundwater discharge. Unfortunately, it was not possible to directly connect this upward discharge to the regional inflow at the eastern boundary as part of the data is below the DOI. However, a flow connection is likely to exist between the lagoon and the inland deep aquifers, thus providing offshore discharge by leakage from deep aquifer systems. This type of leakage could have been made possible by erosion of clay layers from buried valleys, as discussed previously. This hypothesis is further supported by the very low resistivities observed in the "blob" between 12,000 and 14,500 m, as this feature resembles the characteristics of the buried valleys and could stem from seawater left behind in the process of lagoon formation.

Numerical models

Conceptual hydrogeological models

The information from the two boreholes was combined with the geophysical results to conceptualize the hydrogeology at the two cross-sections. Hence, two different conceptual models were built, one to model cross-section A and the second to model cross-section B. Both are 25 km long consisting of 8 km of land east of the lagoon, 12 km of lagoon, 2 km of Holmsland Barrier, and extending 3 km out in the sea (Fig. 4). The depth of the models is 200 m. Confining units observed in the deep borehole at Stauning are shown in Fig. 4a. The borehole at Holmsland Barrier is assumed to be located in a buried valley. Several of such valley incisions are assumed to exist underneath the lagoon (Kirkegaard et al. 2011). The precise location and extent of these and how they have eroded into confining units are not known. Figure 4a,b shows examples of several buried valleys (dashed triangles) that were built into the conceptual model in conjunction with numerical modeling to (1) provide trapping of very old saltwater in defined areas and (2) provide off-shore discharge in agreement with the interpretation of the geophysical data. Based on the geophysical interpretations, saltwater interfaces (SWI) are also shown. The lagoon shoreline is used as a reference for the distance where clay layers are assumed to terminate. The geology of the two models is similar for the shallow aquifers (0–26 meter below sea level, mbsl), but differs significantly in the deeper parts 20–200 mbsl. The termination of the upper two clay layers (10–16 and 26–38 mbsl) is perhaps a result of the two layers pinching out, or alternatively a result of buried valleys incision only to a very shallow depth. Model 'A' (Fig. 4a) suggests that groundwater may flow from shallow aquifers towards the shoreline. Fresh groundwater within deeper aquifers is not interpreted beyond 3,000 m from the shoreline; hence, the confining clay layers at 60–90, 106–131, and 158–169 mbsl observed in borehole DGU 93.1125 are assumed to terminate at the same distance from the eastern shoreline leaving several windows in the clay layers in (Fig. 4a). Model 'B' (Fig. 4b) is different from A in that the buried valleys only erode the top confining layers close to the eastern shoreline restricting SGD from deeper aquifers to occur only far offshore. The clay layers at 60–90 and 106–131 mbsl are still assumed to be cut by buried valleys approximately 4,000 m from the shoreline and to have a window of approximately 500 m length, after which they continue again ~5,000 m, where they are again cut by two buried valleys near the Holmsland Barrier. The clay layer at 158–169 mbsl is left intact below the lagoon.

Homogeneous case: evolution of lagoon salinity and submarine groundwater discharge (SGD)

Figure 5 shows the simulated salinity distribution and groundwater flow patterns at the end of stages I and IV in the case where the subsurface is assumed to be homogeneous. Figure 5a shows the results from 5,000 years ago, when the North Sea coastline was located where the shoreline of the lagoon stands today (17,000 m), i.e., the lagoon did not exist. Figure 5b represents the end of the last stage (IV) with a lagoon (5,000–17,000 m) and after changing the lagoon salinity in three stages over the preceding 300 years. The salinity is plotted relative to the density of seawater and freshwater (that remains the same throughout the simulation). Flow vectors show direction, but not magnitude.

At the end of stage I (Fig. 5a), groundwater flows from land towards the sea. The salinity distribution shows a sharp transition from freshwater to saltwater at the interface creating the characteristic saltwater wedge. The appearance of a very sharp transition in salinity around the saltwater wedge is caused by the vertical exaggeration.

 DOI 10.1007/s10040-014-1195-0

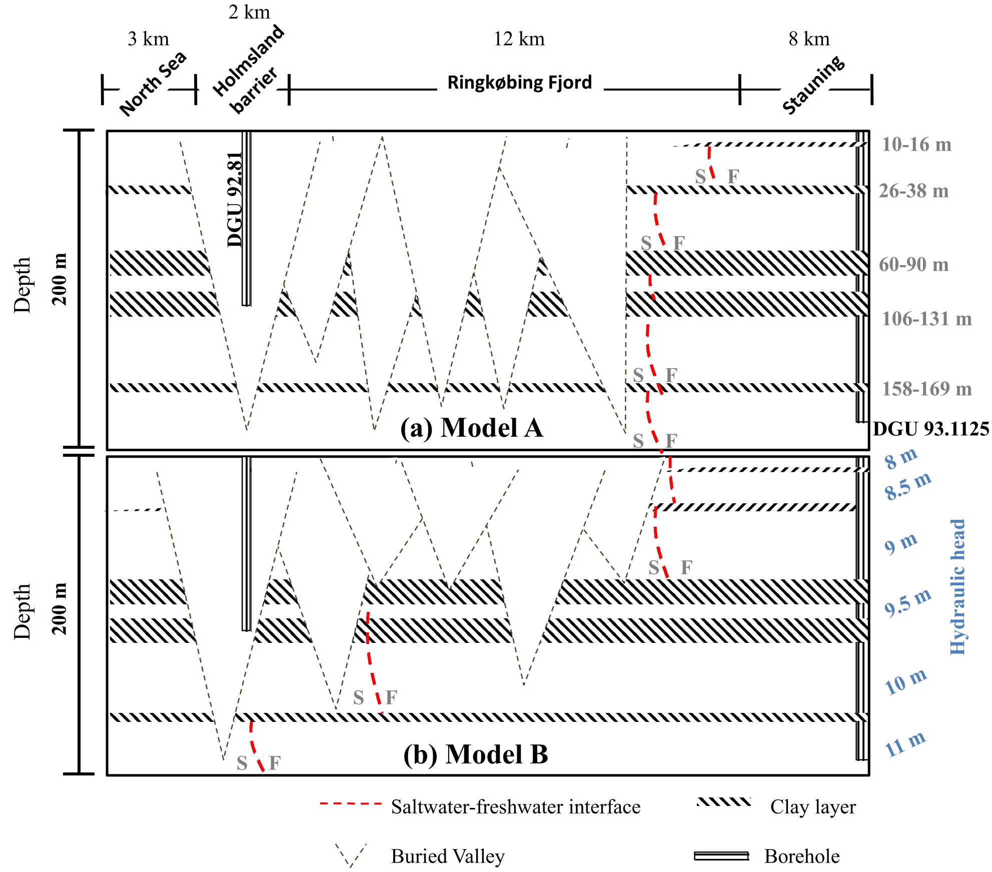

Fig. 4 Conceptual models **a** A and **b** B, showing North Sea, Holmsland Barrier, Ringkøbing Fjord, and landside (Stauning). Both models are based on geophysical inversion cross-sections type 'A' and 'B' including east-borehole (*93.1125*) and west-borehole (*92.133*). *Dotted triangles* show the hypothetical incision of buried valleys into clay layers. The *red dashed lines* are the assumed saltwater–freshwater (S, F) interface location. Hydraulic head for each aquifer is shown in *blue font* in conceptual *model B*. Figure not to scale

Groundwater discharging into the sea near the shoreline is of terrestrial origin in the upper part of the aquifer, whereas groundwater from the deeper parts has mixed with seawater. Flow on the other side of the transitional zone is affected by the seawater recirculation system. Recirculation occupies the entire depth and thus blocks any component of freshwater SGD to offshore parts of the lagoon.

Figure 5b shows the results at the end of the last stage IV, where the North Sea shoreline (3,000 m) is located to the west of the Holmsland Barrier and the salinity and water level of the lagoon (5,000–17,000 m) are controlled via the operation of the Hvide Sande sluice. The flow pattern shows groundwater movement from land towards what is now the lagoon with a sharp transition between freshwater and brackish water. Fresh groundwater has therefore no direct interaction with seawater in the upper part of the aquifer, but mixes with water from the lagoon at greater depth. Flow from the sea towards the lagoon still blocks fresh groundwater from reaching the North Sea. The local circulation at the Western boundary of the lagoon is generated by groundwater recharge at Holmsland Barrier. Flow patterns on the seaside of the transition zone are more complex as compared to stage I. There are large circulation patterns between seawater and lagoon water, as well as localized circulations below the lagoon. The presence of the lagoon has caused brackish water to invade the sediment bed and top of the aquifer over a couple of hundred years. The transitional zone is thus much wider in the upper part of the domain, whereas the toe of saltwater has extruded ~500 m offshore. The simulation suggests two phenomena; the current system is in a transient state where refreshening is still ongoing, and the presence of the lagoon influences the location and width of the transitional zone. Nevertheless, the salinity distribution using a homogeneous geological model compares poorly with the patterns found in Fig. 3.

Heterogeneous cases: evolution of lagoon salinity and SGD

Figure 6 presents conceptual models A and B at the end of stage IV. In case A, all confining layers terminate at around 15,000 m except the upper first confining layer that terminates around 16,500 m. Groundwater flows towards the lagoon shoreline (17,000 m) in the upper part of the domain. With increasing depth, groundwater flows further offshore as a result of the deeper confining layers that terminate further from the lagoon shoreline. Lagoon water has caused extrusion of seawater in the upper aquifer. The

 DOI 10.1007/s10040-014-1195-0

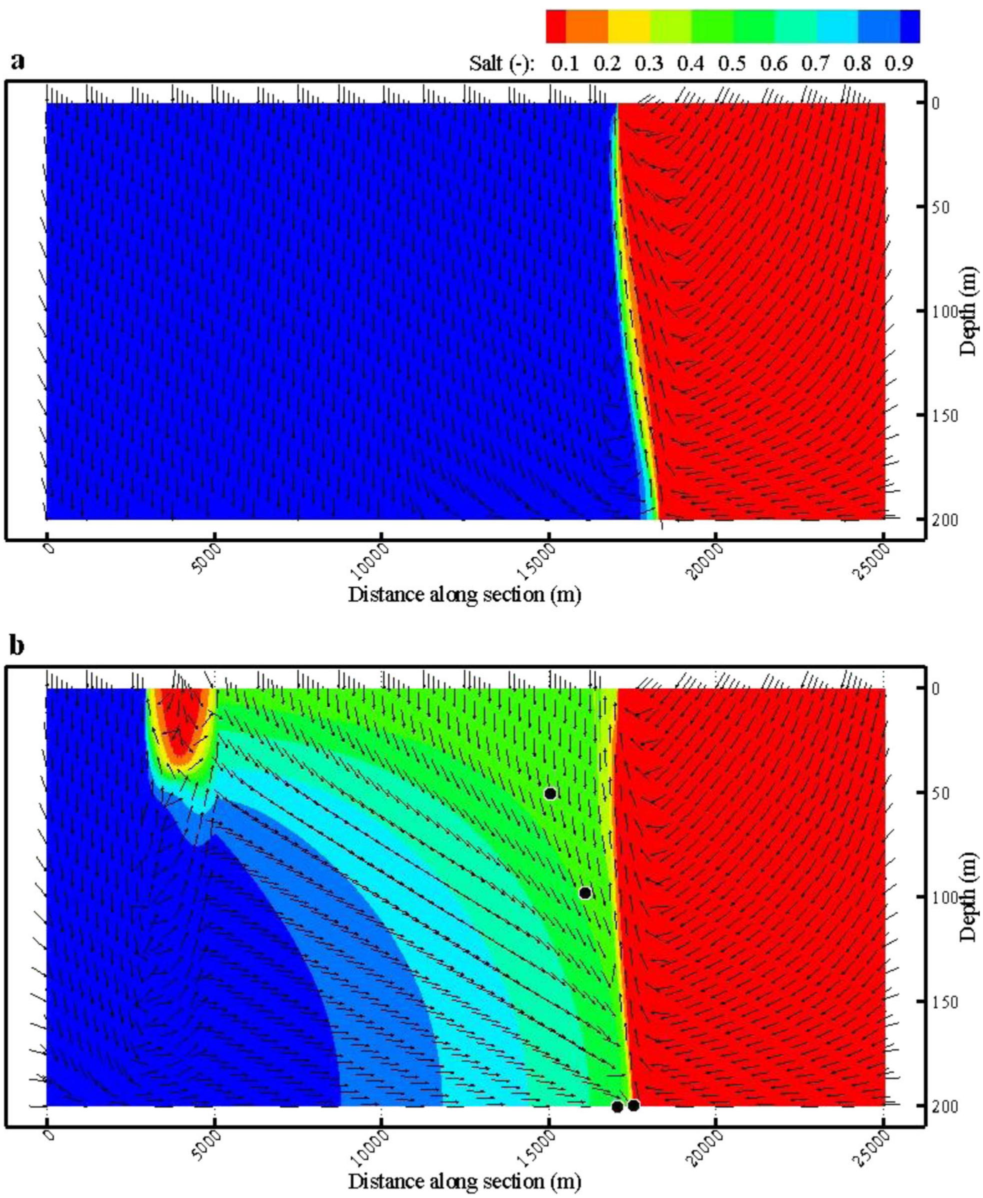

Fig. 5 Homogeneous case simulated under hypothetical evolution of the lagoon showing simulated relative salt distribution and representative flow vectors under **a** no lagoon with sea shoreline after stage I and **b** after stage IV, i.e., lagoon is present under current salinity conditions. Salt distribution is represented as percentage of density relative to density in seawater. *Flow arrows* do not indicate magnitude of groundwater discharge, only direction. *One arrow* is shown for every 75 elements. The *black dots* (**b**) mark the concentration observation points in Fig. 9

simulated salinity distribution resembles better the resistivity distribution observed in cross-section A (Fig. 3a) than that of the homogeneous model. Simulated groundwater exchange with the lagoon (SGD) is shown in Fig. 7, i.e., fluxes across the top face of the domain. Recharge values from the lagoon into groundwater are positive, while discharge from groundwater into the lagoon is negative. The system with confining layers leads to three distinct SGDs into the lagoon; near the shoreline and two offshore (Fig. 7a). The discharge at the lagoon shoreline is around 0.17 m/d. The two offshore discharge peaks reach values of ~0.018 and ~0.05 m/d near 16,750 and 15,050 m, respectively. The two off-shore SGDs cannot be neglected as the relative peaks are 10–30 % of the shoreline SGD, but greater in spatial extent (especially for the peak at 15,050 m, see also the following). There is no SGD into the North Sea from the eastern side of the lagoon; however, some SGD takes place due to recharge at Holmsland Barrier. The very small negative and positive fluxes (discharge and recharge) are local recirculation of groundwater and lagoon water.

The simulated salinity distribution (Fig. 6a) follows the flow and discharge patterns. Low salinities are observed near the discharge points. The freshwater contribution to the shoreline discharge is from the unconfined and the upper confined aquifer. The first and second confined aquifers contribute to the first offshore SGD, while the SGD at the furthest off-shore point is a result of flow from

DOI 10.1007/s10040-014-1195-0

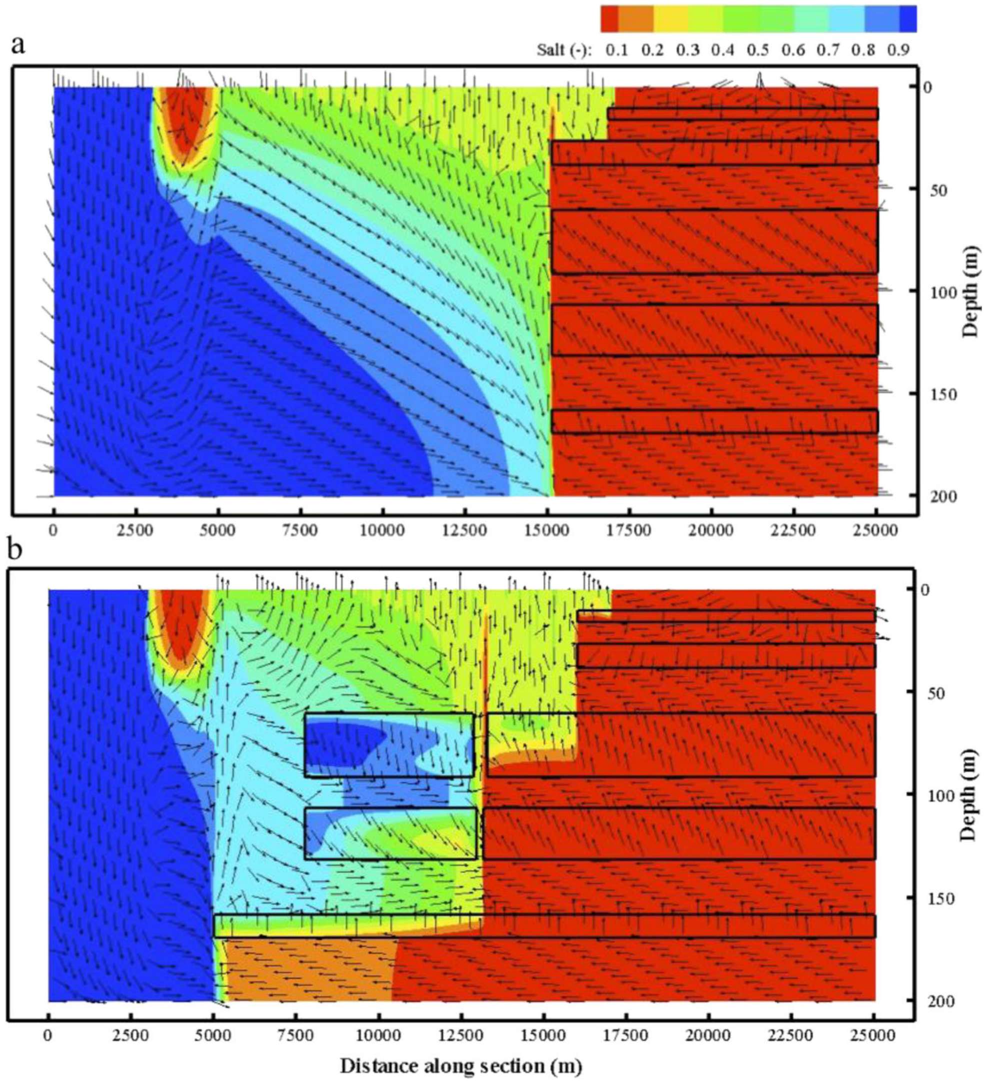

Fig. 6 Heterogeneous cases simulated under hypothetical evolution of the lagoon with the aid of conceptual models 'A' and 'B' after stage IV. **a** Heterogeneous case A and **b** Heterogeneous case B. Salt distribution is represented as percentage of density relative to density in seawater. *Black rectangular blocks* show location of confining units. *Flow arrows* do not indicate magnitude of groundwater discharge, only direction. *One arrow* is shown for every 75 elements

deeper aquifers. Since the salinity of the lagoon water is lower than the sea, a refreshening of the aquifers right below the lagoon has taken place. However, the lagoon loses water even further offshore, which is circulated back to the lagoon at the discharge locations. Likewise, seawater also contributes to SGD into the lagoon, but only at the most offshore discharge point at ~5,000 m (as observed from the flow tube extending from almost the bottom of the domain to the lagoon), resulting in discharge rates that are slightly higher than at the points further east (Fig. 7a). This discharge is generated by recharge at the Holmsland Barrier plus the contribution from the seawater. The recharge from rainfall has formed a freshwater lens below the Holmsland Barrier (3,000–5,000 m). The elevated resistivity signature of the freshwater lens is clearly visible in the cross-sections shown by Kirkegaard et al. (2011); however, for the particular cross sections shown here (Fig. 3), the data acquired over the Holmsland Barrier had to be removed from the dataset because of coupling to manmade installations. The flow vectors at this freshwater lens show a groundwater divide with discharge to the lagoon and sea shoreline. Another groundwater divide is observed around 4 km inland from the lagoon shoreline (21,500 m). The recharge occurring in stage II, III, and IV has resulted in a groundwater divide in the upper part of the domain on the landside (as compared to the homogeneous model). This influence gradually disappears after the first confined aquifer.

In case B, the first two confining layers terminate around 16,000 m, while the fifth one terminates around 5,000 m. The third and fourth confining layers discontinue around 13,500 and 13,250 m, respectively, and then continue again, leaving 'windows' of about 500 and 250 m, respectively, that mimic an incision by a V-shaped buried valley. The flow vectors show groundwater flowing

DOI 10.1007/s10040-014-1195-0

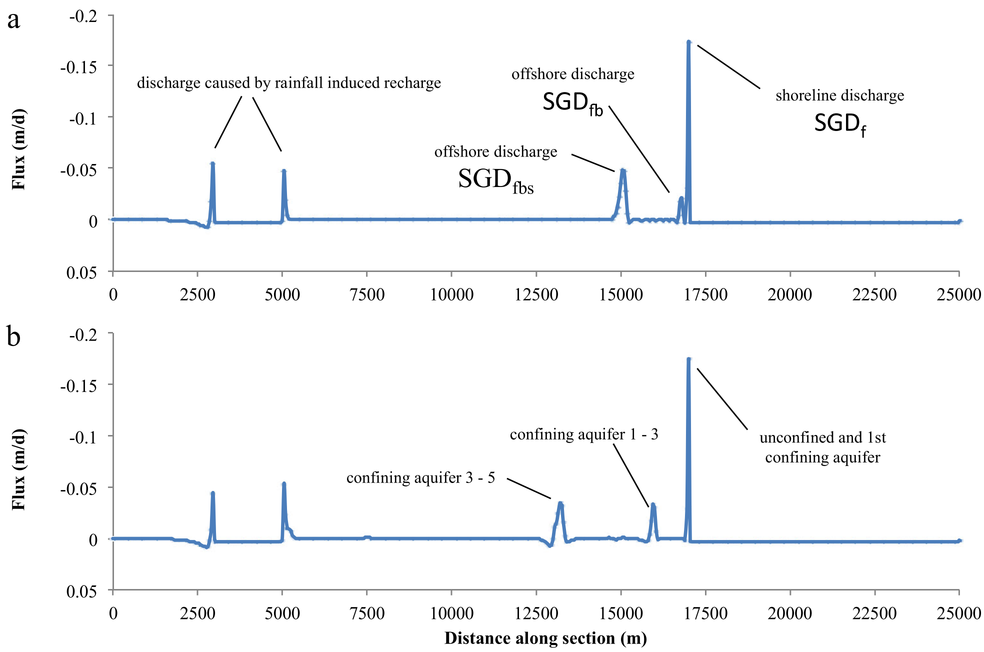

Fig. 7 Groundwater fluxes across the surface of model under **a** heterogeneous case A and **b** heterogeneous case B. *Positive values* represent flux coming into the domain while negative values represent flux leaving the domain. SGD_f, SGD_{fb} and SGD_{fbs} correspond to fresh, fresh+brackish and fresh+brackish+salty components of the SGD, respectively

towards the lagoon shoreline (17,000 m) from the unconfined and the first two confined aquifers. However, for the deeper aquifers, the flow vectors show that groundwater flows further offshore as a result of the presence of the confining layers terminating further away from the shoreline. The windows in the confining layers contribute to SGD into the lagoon through deeper aquifers. Furthermore, SGD from all the deep aquifers contribute to upward far-offshore SGD into the lagoon. The pathway and magnitude of this far-offshore SGD is enough to trap a small zone of old groundwater (old residual seawater) of higher salinity located in the 3rd confining unit between 13,000 and 16,000 m. The recirculation of groundwater appears to slowly dilute this old water. The shift of the sea coastline and subsequent change of salinity in the lagoon has resulted in trapping of this residual seawater in the relatively complex geological setting.

The regional and local seawater recirculation patterns are more complex compared to case A (Fig. 6a). The brackish water distribution under the lagoon is much more variable as a result of greater heterogeneity. In case B, saltwater extrusion extends further offshore because SGD mainly takes place when confining layers terminate or through the small windows caused by incision of buried valleys. The salinity distribution also resembles the resistivity distribution observed in cross-section B (Fig. 3b) in which trapped seawater and offshore discharge was found. Hence, the trapped seawater could be a result of the combination of geology and historical evolution of the lagoon.

Like in case A, there is no SGD to the sea except from the Holmsland Barrier due to recharge. The magnitude of SGD is shown in Fig. 7b. Discharge at the lagoon shoreline is again around 0.17 m/d followed by 0.03 m/d of discharge around 15,950 m, which is controlled by the presence of the first and second confined aquifers. Even further offshore, around 13,200 m, a SGD of 0.03 m/d is found which is controlled by the windows in the third and fourth confining clay layer. The two SGD distributions are similar and cannot be neglected compared to the shoreline SGD. Like in case A, very small fluxes of discharge and recharge are found offshore, which could be local recirculation of groundwater and lagoon water.

Total groundwater input and simulated SGD estimates

From the obtained results, the simulated groundwater fluxes can be divided into three components; the total terrestrial groundwater (Q_t) input from the landside boundary, total net SGD (Q_{sgd}) into the lagoon and total seawater flux (Q_{sea}) entering from the sea boundary into the domain. Q_t entering the lagoon bed from the aquifer system is ~14.5 m^3/d (average of the heterogeneous cases A and B) This corresponds to a flux that is 68 % greater than net precipitation on Ringkøbing Fjord and ~17 % of Skjern River input into the lagoon given a 40-km-long shoreline. The Q_{sgd} estimated into the lagoon averaged from both the heterogeneous cases is ~15.3 m^3/d, which is slightly higher than Q_t since seawater also contributes to this flux. The estimated Q_{sea} component found as the difference between Q_t and Q_{sgd} is thus ~0.8 m^3/d. The simulated Q_{sgd} can be freshwater entering the lagoon from the multi-aquifer system or it may be recirculated brackish and/or seawater, or a combination of all three. Hence, Q_{sgd} is further divided into three components based on three main peaks in the simulated SGD (Fig. 7): freshwater shoreline discharge (SGD_f), fresh–brackish offshore

 DOI 10.1007/s10040-014-1195-0

discharge (SGD_{fb}) and fresh–brackish–salty far-offshore discharge (SGD_{fbs}). The SGD_f is 34 %, SGD_{fb} is 8 % and SGD_{fbs} is 35 % of total Q_{sgd} for case A. A similar analysis was carried out for case B resulting in 33, 15, and 22 % for the same SGD components, respectively. If the SGD_f component is integrated over the entire eastern shoreline a discharge corresponding to ~59 % of the recharge on Ringkøbing Fjord and ~6 % of Skjern River input into the lagoon.

Sensitivity analysis of dispersion and hydraulic conductivity

A sensitivity analysis was carried out for longitudinal dispersivity and hydraulic conductivity using the homogeneous base case; shown here at the end of stage IV (Fig. 8). It was chosen to use the homogeneous case to better assess solely the influence of dispersion. Longitudinal dispersivities of 1, 12.5, 25, 50, and 100 m were tested using a ratio of 0.1 between vertical and longitudinal dispersivity. Figure 8a shows that the simulated 50 % saltwater–freshwater interface moves both at the base of the lagoon and at the toe. The toe extrudes ~ 2 km horizontally with increasing longitudinal dispersivity. The SWI at the base of the lagoon sinks by ~50 m with increasing dispersivity. Groundwater velocity and salinity distribution affect each other, and longitudinal dispersivity is more sensitive when the salt concentration gradient is parallel to the flow direction (data not shown) and vice versa transverse dispersivity is more sensitive where flow (data not shown) is perpendicular to the salt concentration gradient. Hence, these two dispersion components play a role in extruding the toe of the interface and in vertical displacement beneath the lagoon.

The simulated 50 % saltwater–freshwater interface found using a horizontal hydraulic conductivity of 10 m/d was

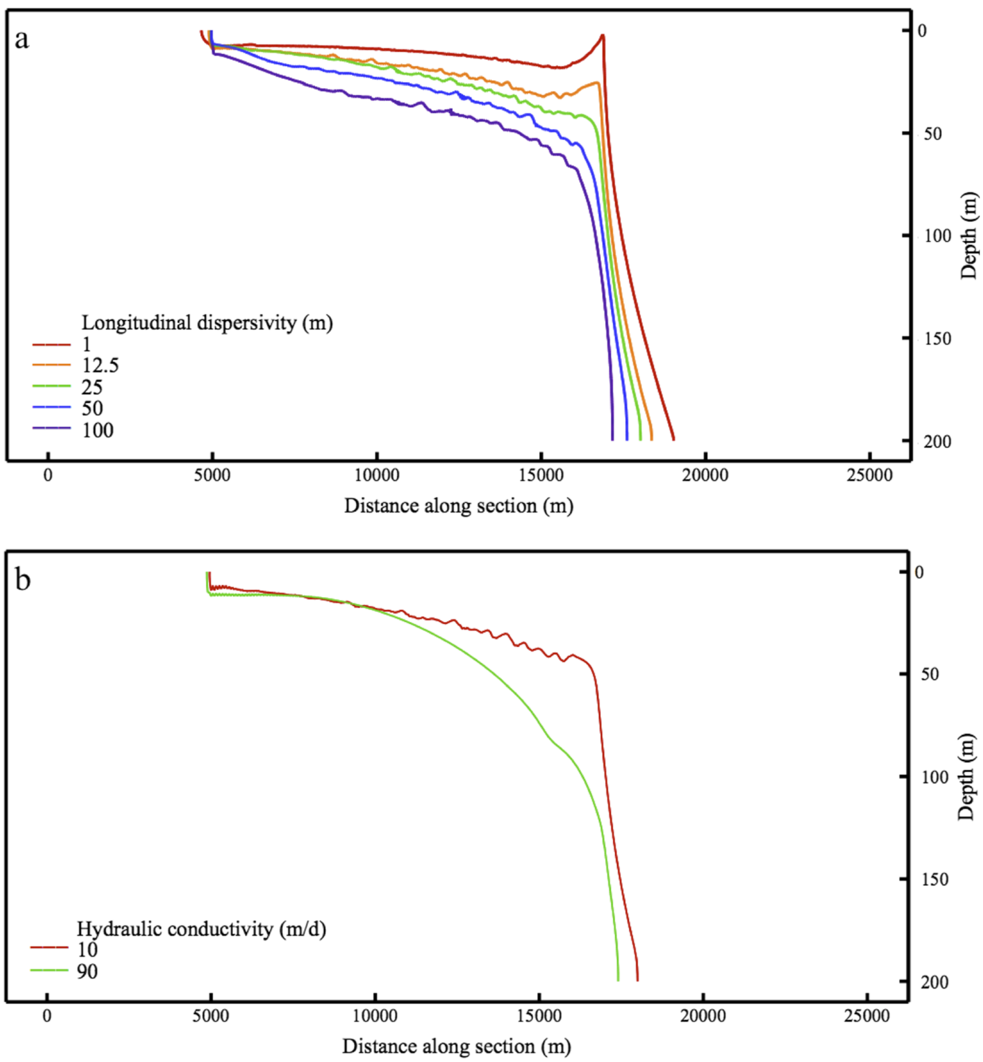

Fig. 8 Sensitivity analysis of the homogeneous model at the end of stage IV. **a** The 50 % saltwater–freshwater interface is shown as a function of longitudinal dispersivity. A value of 25 m is used in the model results shown in Figs. 5 and 6. In all cases, the vertical dispersivity is 10 % of the longitudinal dispersivity. **b** The 50 % saltwater–freshwater interface is shown as a function of horizontal hydraulic conductivity. A value of 50 m/d is used in the models in Figs. 5 and 6. In all cases, the horizontal hydraulic conductivity is 10 % of the vertical hydraulic conductivity

 DOI 10.1007/s10040-014-1195-0

compared to the results obtained using a value of 90 m/d, keeping the vertical hydraulic conductivity an order of magnitude less. Figure 8b shows that an increase in hydraulic conductivity is more important for the location of the saltwater–freshwater interface at the base of the lagoon than at the toe. The toe moves horizontally ~500 m over a model length of 25,000 m, while the interface sinks by up to 50 m in the vertical direction under the lagoon over a model thickness of only 200 m. This is because the groundwater flow direction (data not shown) is mainly horizontal in the upper part of the interface; thus, the horizontal hydraulic conductivity has higher influence which is opposite to the influence of vertical hydraulic conductivity at the toe which is an order of magnitude lower. Additionally, the SGD component around the shoreline is around an order of magnitude higher in the case where a hydraulic conductivity of 90 m/d was used (data not shown). The uncertain architecture of the multi-aquifer system and its parameterization will therefore affect the simulated salinity distribution and resulting SGD.

Salinity distribution in the future

To investigate if the current situation is stable, a simulation for an extra 1,000 years was carried out for the homogeneous case with the lagoon at its current salinity levels. The initial conditions at the end of stage IV were used. The results (Fig. 9) suggest that significant changes will take place in the salinity distribution and SWI. The 75 % salt contour under the lagoon bed sinks vertically by ~50 m and the toe extrudes by ~1,000 m (not shown). This means that extrusion takes place and the width of the transitional zone increases. Hence, the salinity distribution under the lagoon is not at steady state, which is further exemplified by four observation points in the transitional zone (Fig. 9). Observation points are placed at (1) 15,000 m at a depth of 50 m (2) 16,000 m at a depth of 100 m, (3) 17,000 m at a depth of 200 m, and (4) 17,500 m at a depth of 200 m (Fig. 5b). The two latter points are placed around the toe of the saltwater interface. The results show that the concentrations at all four observation points decrease in the future, for some locations for the next 1,000 years under current lagoon salinity. According to the simulations, the system is therefore refreshening, i.e., extruding saltwater. However, the bulk part of the refreshening has taken place during the past 300 years.

Conclusions

The interpreted salinity distribution beneath the Ringkøbing Fjord is complex and the result of (1) historical changes in the development of the lagoon in terms of location and variation in salinity and (2) submarine groundwater discharge from a multi-aquifer sand/clay system incised by sandy buried valleys. A numerical variable-density flow and transport model demonstrates that the multi-aquifer architecture with clay layers terminating below the lagoon or with leakage windows are needed to explain the interpreted salinity distributions (as revealed by resistivity images) such as trapped old seawater and focused discharge of freshwater. A homogeneous model failed in revealing the same features.

The main results are that (1) the groundwater-lagoon system is undergoing refreshening, a process that has been on-going for the past 300 years and will continue, but more slowly, for the next 1,000 years; (2) the multi-aquifer system leads to distinct zones of submarine

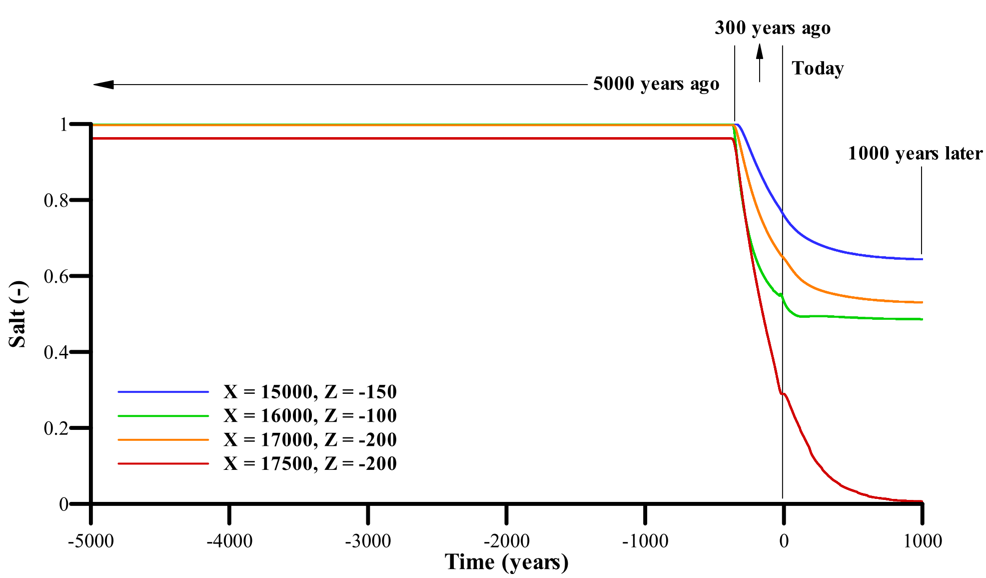

Fig. 9 Changes in concentration at observation points located in the transitional zone within the model domain. The locations of these observation points are shown in Fig. 5b. The past 5,000 years show steady concentration, whereas the concentration has decreased due to evolution of the lagoon during the last 300 years. The lagoon salinity simulated for 1,000 years in the future shows that the system is still under transient conditions

 DOI 10.1007/s10040-014-1195-0

groundwater discharge to the lagoon, near the shoreline, but also offshore as dictated by either the termination of the clay layers or the leakage windows in the clay layers. Offshore discharge zones can be recognized in the resistivity images and the importance of these compared with near the shoreline cannot be neglected. There is no direct interaction with the groundwater system and the sea. On the scale of the lagoon, SGD_f is 59 and 6 % of recharge on the lagoon and the inflow from the river respectively. On the other hand the SGD_{fb} and SGD_{fbs} together amount to 71 and 7 % of recharge on the lagoon and the inflow from the river respectively; therefore, contributions from SGD_f, SGD_{fb}, SGD_{fbs}, i.e. from both shallow and deep aquifers, cannot be neglected, be it near shore or far offshore SGD.

The numerical study demonstrates the importance of including the geomorphological and anthropogenic changes in the landscape (formation of lagoon and operation of the sluice) on the results by changing the boundary conditions over the past ~5,000 years. The study, however, also demonstrates that the parameterization of the multi-aquifer system plays a big role in the simulated salinity distribution, e.g. changes in the hydraulic conductivity or dispersivities result in significant changes in the saltwater–freshwater interfaces.

Finally, this study shows the potential of large-scale airborne geophysical investigations as an excellent tool to map and understand complex geology, salinity distribution, and submarine groundwater discharge. Using geophysical interpretations, regional-scale conceptual models can be designed which can aid in setting up numerical simulations.

Acknowledgements This work was supported by The Research School of Water Resources (FIVA) and HOBE - Center for Hydrology–Hydrological Observatory, which is funded by the Villum Foundation. We also want to thank two anonymous reviewers for their insightful comments which greatly helped improve the manuscript.

References

Andersen MS, Baron L, Gudbjerg J, Gregersen J, Chapellier D, Jakobsen R, Postma D (2007) Discharge of nitrate-containing groundwater into a coastal marine environment. J Hydrol 336:98–114. doi:10.1016/j.jhydrol.2006.12.023

Anthony D, Moller I (2002) The geological architecture and development of the Holmsland Barrier and Ringkobing Fjord area, Danish North Sea Coast. Geografisk Tidsskrift 102:27–36. doi:10.1080/00167223.2002.10649463

Auken E, Christiansen AV, Jacobsen LH, Sørensen KI (2008) A resolution study of buried valleys using laterally constrained inversion of TEM data. J Appl Geophys 65:10–20

Burnett WC, Taniguchi M, Oberdorfer J (2001) Measurement and significance of the direct discharge of groundwater into the coastal zone. J Sea Res 46:109–116. doi:10.1016/S1385-1101(01)00075-2

Burnett WC, Aggarwal PK, Aureli A, Bokuniewicz H, Cable JE, Charette MA, Kontar E, Krupa S, Kulkarni KM, Loveless A, Moore WS, Oberdorfer JA, Oliveira J, Ozyurt N, Povinec P, Privitera AMG, Rajar R, Ramassur RT, Scholten J, Stieglitz T, Taniguchi M, Turner JV (2006a) Quantifying submarine groundwater discharge in the coastal zone via multiple methods. Sci Total Environ 367:498–543. doi:10.1016/j.scitotenv.2006.05.009

Burnett WC, Dulaiova H, Stringer C, Peterson R (2006b) Submarine groundwater discharge: its measurement and influence on the coastal zone. J Coastal Res S1(39):35–38

Carter ES, White SM, Wilson AM (2008) Variation in groundwater salinity in a tidal salt marsh basin, North Inlet Estuary, South Carolina. Estuar Coast Shelf S 76:543–552. doi:10.1016/j.ecss.2007.07.049

Cohen D, Person M, Wang P, Gable CW, Hutchinson D, Marksamer A, Dugan B, Kooi H, Groen K, Lizarralde D, Evans RL, Day-Lewis FD, Lane JW Jr (2010) Origin and extent of fresh paleowaters on the Atlantic continental shelf, USA. Ground Water 48:143–158. doi:10.1111/j.1745-6584.2009.00627.x

Friborg R, Thomsen S (1999) Kortlægning af Ribe Formationen (Mapping of Ribe Formations). Et fællesjydsk grundvandssamarbejde [Mapping the Ribe Formation: a cooperate groundwater investigation project]. Vejle og Sønderjyllands Amt Populær rapport, Ribe, Ringkjøbing, Viborg, Arhus, Denmark

Johansen AC (1913) Om Forandringer i Ringkøbing Fjords Fauna [About changes in Ringkøbing Fjord Fauna]. Kommissionen for Havundersøgelser, Denmark, Bianco Lunos, Copenhagen

Jørgensen F, Sandersen PB (2006) Buried and open tunnel valleys in Denmark: erosion beneath multiple ice sheets. Quat Sci Rev 25:1339–1363

Jørgensen F, Sandersen PB (2009) Buried valley mapping in Denmark: evaluating mapping method constraints and the importance of data density [Kartierung eiszeitlicher Rinnen in Dänemark: Bewertung methodischer Grenzen und Bedeutung der Datendichte]. Z Dtsch Ges Geowiss 160:211–223

Jørgensen F, Sandersen PB, Auken E, Lykke-Andersen H, Sørensen K (2005) Contributions to the geological mapping of Mors, Denmark: a study based on a large-scale TEM survey. Bull Geol Soc Den 52:53–75

Kaleris V, Lagas G, Marczinek S, Piotrowski JA (2002) Modelling submarine groundwater discharge: an example from the western Baltic Sea. J Hydrol 265:76–99

Kirkegaard C, Sonnenborg TO, Auken E, Jorgensen F (2011) Salinity distribution in heterogeneous coastal aquifers mapped by airborne electromagnetics. VZJ 10:125–135. doi:10.2136/vzj2010.0038

Langevin CD (2003) Simulation of submarine ground water discharge to a marine estuary: Biscayne Bay, Florida. Ground Water 41:758–771. doi:10.1111/j.1745-6584.2003.tb02417.x

Manheim FT, Krantz DE, Bratton JF (2004) Studying ground water under Delmarva coastal bays using electrical resistivity. Ground Water 42:1052–1068. doi:10.1111/j.1745-6584.2004.tb02643.x

Nielsen MH, Rasmussen B, Gertz F (2005) A simple model for water level and stratification in Ringkobing Fjord, a shallow, artificial estuary. Estuar Coast Shelf S 63:235–248. doi:10.1016/j.ecss.2004.08.024

Post VEA, Van der Plicht H, Meijer HAJ (2003) The origin of brackish and saline groundwater in the coastal area of the Netherlands. Neth J Geosci 82:133–147

Post VEA, Vandenbohede A, Werner AD, Maimun TMD (2013) Groundwater ages in coastal aquifers. Adv Water Resour 57:1–11. doi:10.1016/j.advwatres.2013.03.011

Rasmussen ES (2004) Stratigraphy and depositional evolution of the uppermost Oligocene–Miocene succession in western Denmark. Bull Geol Soc Den 51:89–109

Robinson C, Gibbes B, Li L (2006) Driving mechanisms for groundwater flow and salt transport in a subterranean estuary. Geophys Res Lett 33. doi:10.1029/2005GL025247

Santos IR, Niencheski F, Burnett W, Peterson R, Chanton J, Andrade CFF, Milani IB, Schmidt A, Knoeller K (2008) Tracing anthropogenically driven groundwater discharge into a coastal lagoon from southern Brazil. J Hydrol 353:275–293. doi:10.1016/j.jhydrol.2008.02.010

Scharling PB, Rasmussen ES, Sonnenborg TO, Engesgaard P, Hinsby K (2009) Three-dimensional regional-scale hydrostratigraphic modeling based on sequence stratigraphic methods: a case study of the Miocene succession in Denmark. Hydrogeol J 17:1913–1933

Sørensen KI, Auken E (2004) SkyTEM: a new high-resolution helicopter transient electromagnetic system. Explor Geophys 35:191–199

Spruill TB, Bratton JF (2008) Estimation of groundwater and nutrient fluxes to the Neuse River estuary, North Carolina. Estuar Coast 31:501–520. doi:10.1007/s12237-008-9040-0

Stieglitz T, Rapaglia J, Bokuniewicz H (2008) Estimation of submarine groundwater discharge from bulk ground electrical conductivity measurements. J Geophys Res-Oceans 113. doi:10.1029/2007jc004499

Stisen S, Sonnenborg TO, Hojberg AL, Troldborg L, Refsgaard JC (2011) Evaluation of climate input biases and water balance issues using a coupled surface-subsurface model. VZJ 10:37–53. doi:10.2136/Vzj2010.0001

Therrien R, McLaren RG, Sudicky EA, Panday SM (2004) Hydrosphere: a three-dimensional numerical model describing fully-integrated subsurface and surface flow and solute transport. Université Laval, Quebec City, QB, University of Waterloo, Waterloo, ON, 275 pp

Thompson C, Smith L, Maji R (2007) Hydrogeological modeling of submarine groundwater discharge on the continental shelf of Louisiana. J Geophys Res-Oceans 112. doi:10.1029/2006jc003557

Vaeret L, Leijnse A, Cuamba F, Haldorsen S (2012) Holocene dynamics of the salt–fresh groundwater interface under a sand island, Inhaca, Mozambique. Quatern Int 257:74–82. doi:10.1016/j.quaint.2011.11.020

Vest Christiansen A, Auken E (2012) A global measure for depth of investigation. Geophysics 77:WB171–WB177

Viezzoli A, Tosi L, Teatini P, Silvestri S (2010) Surface water-groundwater exchange in transitional coastal environments by airborne electromagnetics: the Venice Lagoon example. Geophys Res Lett 37. doi:10.1029/2009gl041572

Vrbancich J (2009) An investigation of seawater and sediment depth using a prototype airborne electromagnetic instrumentation system: a case study in Broken Bay, Australia. Geophys Prospect 57:633–651. doi:10.1111/j.1365-2478.2008.00762.x

Wilson AM (2005) Fresh and saline groundwater discharge to the ocean: a regional perspective. Water Resour Res 41. doi:10.1029/2004wr003399

 DOI 10.1007/s10040-014-1195-0